Structure of phase-separated athermal colloid-polymer systems in the protein limit

Nathan A. Mahynski, Barry Irick, and Athanassios Z. Panagiotopoulos*
Department of Chemical and Biological Engineering, Princeton University, Princeton, NJ 08540, USA
(Received 13 January 2013; published 27 February 2013)

Structural features of phase-separated athermal colloid-polymer mixtures in the so-called "protein limit," where polymer chain dimensions exceed those of the colloid, are investigated using grand canonical Monte Carlo simulations on a fine lattice. Previous work [N. A. Mahynski *et al.*, Phys. Rev. E **85**, 051402 (2012)] has shown that this model accurately captures the phase behavior of experimental systems, and that colloids with sufficiently small diameters, σ_c, relative to that of the monomeric segments, σ_s, phase separate more readily than their large-diameter counterparts. In the present study, we directly connect colloid and polymer structure with their phase behavior by investigating these solutions along their binodal curves; we also explore the role of colloid surface curvature in destabilizing such solutions. Our findings suggest that simple consideration of an additional depletion radius, on the order of the σ_s, leads to a quantitatively accurate prediction of the division between stable and unstable ranges of $d = \sigma_s/\sigma_c$. We compare these results to continuum models with different bonding potentials between monomer segments in order to elucidate the significance of the lattice model's bond fluctuations and inherently coarse colloid surface. In a number of cases, the continuum models deviate both qualitatively and quantitatively from the lattice results, but the binodals of the continuum models are presently not known, making a strong conclusion about these differences impossible.

DOI: 10.1103/PhysRevE.87.022309 PACS number(s): 64.70.pv, 64.70.km, 64.75.Gh

I. INTRODUCTION

Colloid-polymer systems are common in industrial products such as inks, paints, foams, and surfactants [1]. These systems are of particular interest because they serve as a convenient model to study depletion interactions, which also play a considerable role in biological settings, contributing to protein folding, fiber bundling, and the formation of supramolecules [2–5]. Depletion arises as two or more confining surfaces approach one another and exclude a region between them where the depletant, in this case polymer, can no longer exist. This produces an osmotic pressure difference between the bulk and the locally depleted region, which results in an effective attraction that can be strong enough to induce phase separation into colloidal "liquid" and "vapor" phases [5,6]. Fluid phase behavior in colloid-polymer systems is typically characterized by the macroscopic ratio, $q_r = 2R_g/\sigma_c$, where R_g is the average radius of gyration of the polymer in its pure dilute state, and σ_c is the colloid diameter.

Much prior work has been devoted to describing this behavior for systems in the so-called "colloid limit," where $q_r < 1$ [5–15]; in this limit, many coarse-grained descriptions of the polymer are reasonably successful despite neglecting the internal conformational degrees of freedom associated with the polymer chain. In the "protein" limit, $q_r > 1$, such approaches begin to fail as the overall free energy of the system becomes sensitive to details of the polymer. A previous study of the phase behavior of lattice colloids and linear chains demonstrated that proposed rescaling arguments involving the polymer correlation length, ξ, qualitatively failed to collapse the colloid-rich portion of the binodal in the protein limit [16]; this observation had not been previously captured in simulation or analytical models, which suggested such a collapse should be possible [17–19]; however, it is consistent with recent experimental findings [20].

Remarkably, results from Ref. [16] were in near quantitative agreement with experimental binodals, demonstrating the influence of another characteristic length scale in the protein limit, $d = \sigma_s/\sigma_c$, where σ_s is the diameter of a monomer segment [16,21]. These clearly showed that for athermal systems with monomer-monomer excluded volumes, critical densities for $d < 0.25$ collapse to a uniform master curve under rescaling arguments; however, for $d \geqslant 0.25$ at identical q_r, the solutions start demixing at much lower concentrations. McMillan-Mayer-type approaches have suggested this may be due to many-body effects [22,23], but to our knowledge simulations supporting this claim have not yet been performed in the protein limit. In Ref. [16] we postulated that the quantitative improvements observed in that study stemmed from the use of a finely discretized lattice, in which each site interacts with 26 nearest neighbors (coordination number, $z = 26$), rather than the more commonly used $z = 6$. This has significant implications for allowable polymer configurations. "Corner" neighbors on such a lattice give rise to bond lengths of $\sqrt{2}$ and $\sqrt{3}$, fluctuating without an energy penalty. Consequently there is a degree of bond compressibility built into this model that is not present in the lower coordination case where bond lengths are uniformly 1.

In the present study, we examine the structure of colloid-polymer systems over a range of q_r and d values along the binodal curves for the $z = 26$ lattice model of Ref. [16] in an effort to characterize the structure of these systems at coexistence and to clarify the significance, if any, of bond compressibility. We also examine continuum models at the same densities although their binodals are unknown. Additionally, we seek an explanation for the dramatic instability previously observed for sufficiently small colloids. We find a range of diverse structural features that emerge on different sides of these binodals as q_r is increased, illustrating the nontrivial contribution polymer internal degrees of freedom have on the overall free energy

*azp@princeton.edu

of the system. While there have been theoretical attempts to treat such systems at coexistence with liquid-state integral equation theory [24–26], such theories can predict only the spinodal curve, rather than the binodal. Due to computational limitations, previous simulations have also not been able to capture structural details of large many-body systems, nor have they been explicitly linked to phase behavior as they are often at the limit of either one or two colloids [27,28], or have restricted colloid translational degrees of freedom such as in quenched matrices [29].

The rest of this paper is organized as follows. In Sec. II we describe our methodology for both the lattice and continuum models we employ, and describe the metrics used to quantify relevant structural characteristics of the colloid-polymer mixtures. Section III illustrates the results for the fine lattice model at a variety of q_r and d along their respective binodal curves. Finally, Sec. IV qualitatively addresses the influence of bond compressibility by contrasting the results from the fine lattice with those of continuum models.

II. METHODS

We examine the structure of the colloid-polymer systems for both a fine lattice ($z = 26$) and in continuum space. All interactions are athermal, that is, all species interact with one another through a hard sphere potential in continuum space, or by site exclusion on the lattice. Lattice colloids exclude all sites within a radius of $\sigma_c/2$ of their centers, while polymers are modeled as linear chains of beads each occupying a single lattice site ($\sigma_s \equiv 1$). This is representative of fully flexible polymers in a good solvent; while we may envision the beads as either monomers or Kuhn segments, we adopt the convention of referring to these segments as monomers in the rest of this report. In order to examine a range of macroscopic, q_r, and microscopic, d, length scales we employ a similar grid of parameters as previously investigated for phase behavior [16] in Table I. It has been shown that $d \leqslant 0.125$ is representative of the large-diameter (low-curvature) limit, while $d = 0.25$ exhibits instabilities associated with increased curvature. In this way we contrast the effect of d in both limits at constant q_r as illustrated along the diagonals of Table I. Chain lengths have been estimated based on the desired q_r according to their dilute scaling relationship, $R_g = 0.508M^{0.588}$, which has been previously verified for this lattice even at very short chain lengths [16]. Due to discrete chain lengths, it is not possible to exactly reproduce identical q_r values; the target values were $q_r = 1,2$, and 4, which are used as shorthand references henceforth.

We performed grand canonical Monte Carlo (MC) simulations at chemical potentials corresponding to four tie lines we selected; two such tie lines are indicated explicitly in

TABLE I. The macroscopic, $q_r = 2R_g/\sigma_c$, and microscopic, d, size ratios for the lattice systems studied.

		Chain length, M			
σ_c	$d = \sigma_s/\sigma_c$	10	33	110	350
4	0.25	0.984	1.985	4.029	
8	0.125		0.992	2.014	3.978

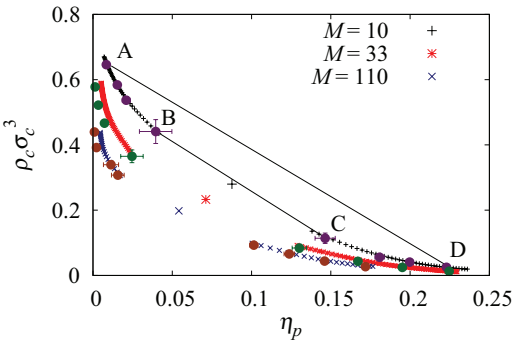

FIG. 1. (Color online) Binodal curves for $\sigma_c = 4$, based on data from Ref. [16]. Large circles indicate the locations of the points sampled along the binodals in the present work, and two tie lines are shown as guides to the eye. 95% confidence intervals are reported when they are larger than symbol size. The abscissa is the monomer concentration, $\eta_p = M\rho_p$, where ρ_p is the polymer number density.

Figs. 1 and 2, with equilibrium points listed alphabetically in order of decreasing colloid density. This alphabetic naming scheme is adopted for all colloid diameters and chain lengths in this report. Only two tie lines are explicitly drawn since all properties we measured varied smoothly between them; in the interest of brevity we often present only the data corresponding to these two lines for each set of size ratios. These coexistence chemical potentials were obtained previously through the use of histogram reweighting as described elsewhere [16]. Monte Carlo moves included local displacements of the colloid by one lattice site, and insertion and deletion of both species, in which Rosenbluth sampling was employed for the polymer [30]. Systems were initialized from configurations on the desired side of the binodal, and care was taken to ensure that only that side was sampled over the course of the simulation. Typical simulations lasted between 50×10^6 and 1×10^9 steps, with a previously optimized ratio of moves. In order to ensure ergodic sampling of system configurations, simulations were run for long enough to ensure that the component of the system with the largest volume fraction reached a ratio of total number of successful insertions and deletions to the average number of that species in the box of at least 1×10^3. Therefore, each of the 1×10^3 snapshots of the system that were collected over the course of the simulation may be taken as independent configurations. Simulation for additional steps

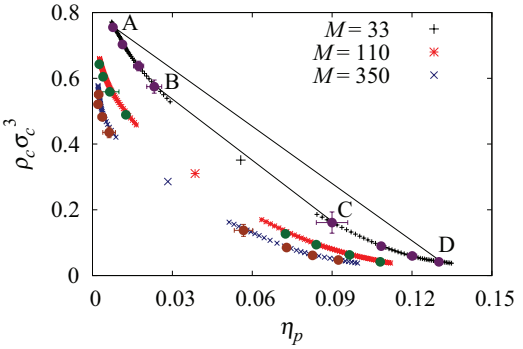

FIG. 2. (Color online) Binodal curves for $\sigma_c = 8$, based on data from Ref. [16]. Symbols, lines, and error bars are the same as Fig. 1.

did not change any measured properties significantly. In each case, the box size was sufficiently large so that no measured property exhibited features at distances greater than half of the box length.

Two related continuum models were also simulated using molecular dynamics (MD) simulations for comparison with the lattice model. We used the HOOMD (Highly Optimized Object-oriented Many-particle Dynamics) package [31,32], which takes advantage of graphics processing units (GPUs) to accelerate the simulation of large systems [33]. All athermal interactions were approximated through the use of a Lennard-Jones potential cutoff at the minimum, $U_{i,j}(r) = 4\epsilon[(\frac{1}{r-\Delta_{i,j}})^{12} - (\frac{1}{r-\Delta_{i,j}})^{6}]$ for $r < r_{\rm cut} + \Delta_{i,j}$, and zero elsewhere. We define $r_{\rm cut} = 2^{1/6}$ and $\Delta_{i,j} = (\sigma_i + \sigma_j)/2 - 1$, so that all particles interact with an identical purely repulsive force independent of particle size. We set the reduced temperature to $k_{\rm B}T/\epsilon = 1.0$. This value has been shown to reproduce hard sphere behavior for symmetric spheres [34].

The first continuum model, the "fixed-bond" model, uses a harmonic bond potential between polymer beads with a coefficient $k = 500$: $U_{\rm fixed\ bond}(r) = \frac{1}{2}k(r - \sigma_s)^2$. Compared to the second model it has a large energy penalty associated with bond length fluctuations away from its equilibrium size. The second model, which we will refer to as the 'free-bond' model, has a shallow bonding potential, allowing the bonds to fluctuate essentially without an energy penalty between 1 and $\sqrt{3}$, which are the limits imposed in the lattice model: $U_{\rm fixed\ bond}(r) = k_f(r - \frac{1+\sqrt{3}}{2})^{16}$. With a value of $k_f = 1 \times 10^8$ this can be integrated with timesteps similar to those required for the Lennard-Jones bead-bead potential. Thus, we can directly contrast the structural effects, if any, due to freely fluctuating bonds.

A Nosé-Hoover thermostat with a coupling constant, $\tau = 1$, was found to equilibrate the system quickly, yielding stable runs at long times. Each MD simulation was run for 300×10^6 steps, with a snapshot taken every 1×10^6 steps. The time step was varied as necessary to give stable results, but in general varied between 0.001 and 0.004 reduced time units. MD simulations were performed at average number densities near the binodal curves obtained from the MC simulations on the lattice.

Polymer structure was quantified through two metrics: the gyration tensor, $\vec{S}$, and the second Legendre polynomial, P_2. The gyration tensor for a chain of length, M, is

$$S_{i,j} = \frac{1}{M}\sum_{k=1}^{M}\left(x_i^k - x_i^{\rm ave}\right)\left(x_j^k - x_j^{\rm ave}\right), \qquad (1)$$

where $\vec{x}^k = \langle x_1^k, x_2^k, x_3^k\rangle$ are the Cartesian coordinates of bead k. Diagonalization of this tensor leads to three eigenvalues, λ_i, which give the three principal axes of the polymer. The square of the radius of gyration is obtained from the sum of these eigenvalues, $\langle R_g^2\rangle = \sum_{i=1}^{3}\lambda_i$. The orientation of each axis relative to a colloid surface is quantified via the second Legendre polynomial, defined as

$$P_{2,i} = \frac{1}{2}\left(3\cos^2\theta_i - 1\right), \qquad (2)$$

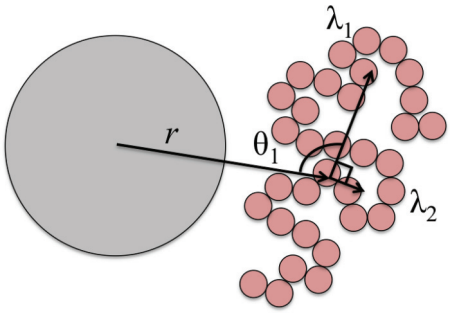

FIG. 3. (Color online) A two-dimensional schematic projection of a polymer in the vicinity of a colloid.

where θ_i is the angle formed by the vector between centers of mass of a polymer and a colloid, and the vector starting at the polymer center of mass extending along λ_i. Thus we obtained three polynomials, $P_{2,i}$, which describe the orientation of each semiaxis of the polymer relative to a colloid surface. A value of $+1$ reflects an orientation of 180°, while a value of -0.5 corresponds to an angle of 90°; random orientations average to a value of 0. Figure 3 illustrates a projection of these metrics into two dimensions, though, of course, our simulations are three dimensional and have an additional eigenvector pointing out of the plane of the page. In this work, we focus our attention on the behavior of the largest semiaxis, $P_{2,1}$. Furthermore, we compare our models by examining the effective monomer depletion layer thickness around the colloids, δ, which may be calculated from the pairwise correlation function:

$$\frac{4\pi}{3}\left[\left(\frac{\sigma_c}{2} + \delta\right)^3 - \left(\frac{\sigma_c}{2}\right)^3\right] = 4\pi\int_{\sigma_c/2}^{\infty} r^2[1 - g_{c,m}(r)]\,dr. \qquad (3)$$

In what follows, errors are calculated by blocking measurements into 10 independent subsets to generate 95% statistical confidence intervals. Measurements that could not be blocked as such, owing to the rarity of such a configuration, are not shown as their statistical error is too large ($\geqslant 30\%$ of the mean value) to be of any statistical significance.

III. LATTICE MODEL

We begin with the results from the fine lattice. Quantities are commonly plotted with an abscissa of $l = (r - \sigma_s)/\sigma_c = r/\sigma_c - d$, which we refer to as the "reduced distance" (cf. Fig. 3). We do so because the locations of key structural features for all d collapse nicely when plotted against this quantity, which conveniently takes into account *both* the colloid and monomer length scales. This collapse is illustrated with dashed lines on figures as appropriate.

As a reference, we first examine the structure at $q_r = 1$. Figure 4 illustrates the average radius gyration for $\sigma_c = 8$, $M = 33$ as a function of the distance between the center of mass of a colloid and that of a polymer, averaged over all configurations. The location of the first peak does not appear to depend on the position along the binodal (density) and remains constant at roughly the radius of the colloid; as a colloid penetrates a polymer coil's core it expands the polymer by roughly 30% over its bulk dimensions. The

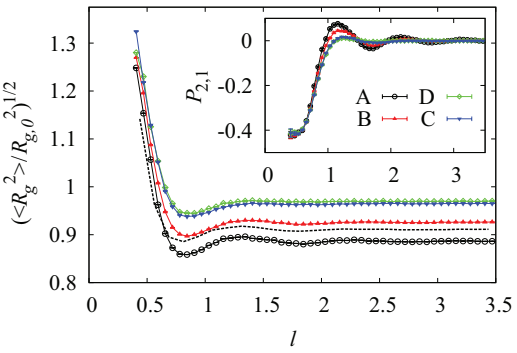

FIG. 4. (Color online) The average radius of gyration of polymers normalized by the values in Table I, and $P_{2,1}$ as a function of reduced distance, l, between their center of mass and neighboring colloids for $\sigma_c = 8$, $M = 33$ ($q_r = 1$). The dashed black line is the result at point A for $\sigma_c = 4$ and $q_r = 1$; while the magnitudes vary, the location of the features align nicely with the results for $\sigma_c = 8$.

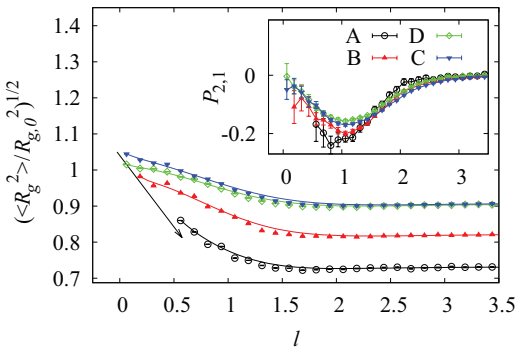

FIG. 5. (Color online) Average radius of gyration of polymers, normalized by the values in Table I, and preferential orientation, $P_{2,1}$, for the case of $\sigma_c = 4$, $M = 110$ ($q_r = 4$). Larger coils show decreasing long-range effects but with increasing colloid density, the peak in R_g is shifted to greater distances as colloids are increasingly expelled from the core.

curves along the polymer-rich branch of the binodal (C, D), are nearly indistinguishable from one another; however, with increasing colloid density along the opposite branch (A, B), it is clear that the polymers become increasingly compressed. Along the polymer-rich branch, the polymer is semidilute and is thus characterized by a meshwork, while along the polymer-lean branch it is far more dilute. As previously shown, the polymer-rich branch can be collapsed using scaling arguments based on correlation length, yet such arguments fail for the polymer-lean branch [16]. Thus, where the binodal collapses based on polymer scaling, polymer dimensions remain independent of density. However, along the polymer-lean branch a clear oscillatory trend with a period of roughly $2R_g$ emerges, progressively increasing in amplitude as colloid density increases. This is also evident for the case of $\sigma_c = 4$ ($d = 0.25$). Results for point A are indicated by the dashed line in Fig. 4; the location of the maxima and minima are consistent with the results for $\sigma_c = 8$, though the overall magnitude of compression is less for the smaller colloids.

Similar trends appear in the inset of Fig. 4 for $P_{2,1}$; again these curves collapse for the polymer-rich branch of the binodal (C, D). Near the colloids, the largest semiaxis rotates almost perfectly tangential to the surface ($P_{2,1} < -0.4$) in what is known as the "docking transition" [27,35,36], whereupon the polymer becomes further distended. Remarkably, this effect occurs in equal magnitude for both halves of the binodal, independent of density. However, only for the colloid-rich branch are additional long-range effects observed. In fact, around a given colloid at least three coherent "shells" are clearly visible. In each of these shells, the polymer displays a weak preference to orient normal to the colloid surface ($P_{2,1} < 0$). As a polymer moves between these shells, however, the trend is reversed, exhibiting a weak preference to orient its longest semiaxis parallel to the outward normal vector from the surface ($P_{2,1} > 0$). These trends become stronger as colloid density increases.

However, with increasing q_r these effects quickly disappear. Once q_r reaches 4, only local effects in the vicinity of the colloid surface remain. Figure 5 illustrates this point; as we push further into the protein limit, the distortion of the chain dimensions and orientations now occurs only for polymers whose center of mass have engulfed colloids ($l < q_r/2 - d = 1.75$); this is accompanied by a significant reduction in the orientational preference trends observed for smaller chain lengths. As colloids approach the core of a polymer coil, $P_{2,1}$ displays a minimum at $l \approx 1$, that is, halfway between the center and perimeter of the coil for $q_r = 4$. As a colloid approaches a polymer coil's core, the relative orientation begins to randomize. This is simply a result of the fact that small fluctuations in chain orientation much more drastically impact the angle between the semiaxes of the polymer and the vector connecting their centers of mass, the latter of which is now quite small. For the polymer-rich branch of the binodal, chain size remains essentially independent of colloid density, while for the colloid-rich branch, increasing density compresses the coils and shifts the peak in Fig. 5 toward the perimeter of the coil. This may be understood through an osmotic compression mechanism, as follows. In general, the compression of a polymer chain at sufficiently high colloid density derives from a polymer coil's entropic expulsion of the colloid species from its core. This creates an osmotic pressure difference between the center of the coil and the bulk, which progressively compresses the coil as overall colloid density (osmotic pressure) increases [37,38]. When q_r is large the net volume occupied by the monomers in a chain comprises a very small fraction of the total coil volume [39]. As the coils progressively compress along the colloid-rich branch of the binodal, their internal density increases, making further invasion by the colloid species less and less favorable. This drives any invading colloids from the center of the chain toward the surface of the coil causing the peak in Fig. 5 and the lower bound of the curves in the inset of Fig. 6 to shift to larger distances from the core. Measurements could not be made reliably at distances shorter than those illustrated in the figures and are omitted for clarity. This effect is most pronounced for large q_r where the chain can accommodate the colloid species closer to its center of mass when sufficiently dilute (cf. Fig. 4). Regardless of q_r or d, the ratios of the gyration tensor's eigenvalues in the bulk were roughly 12:3:1, and remained constant both during compression and across phase boundaries. This is in excellent agreement with data in

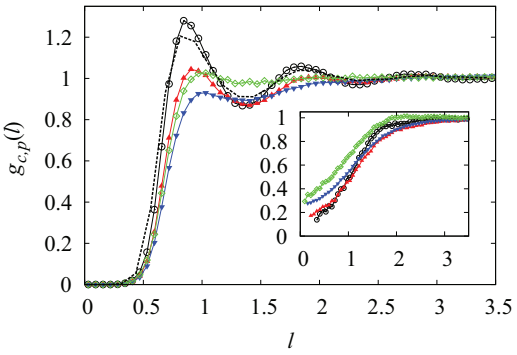

FIG. 6. (Color online) Colloid-polymer-center-of-mass pair correlation function for $\sigma_c = 8$, $q_r = 1$ and 4 (inset). Error bars are small and omitted for clarity. Symbols are the same as in Fig. 5; the dashed black line is the result at point A for $\sigma_c = 4$ and $q_r = 1$.

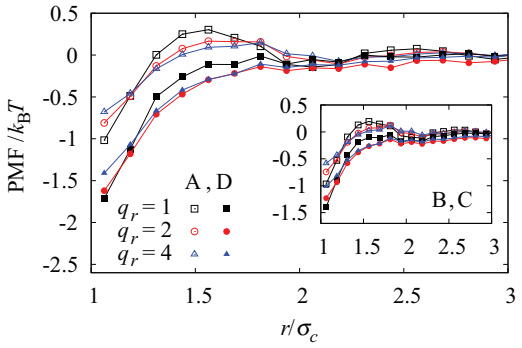

FIG. 7. (Color online) Potential of mean force (PMF) between colloids for $\sigma_c = 8$ far from the critical point (A and D, main plot) and as they approach it (B and C, inset) for all q_r investigated. As the critical point is approached the PMF on both sides of the binodal approaches as value of -1, while further away the halves of the binodal split. Open and closed symbols correspond to the polymer-lean and polymer-rich phases, respectively.

Ref. [40] reported for random walks, as well as simulations involving only a single colloid at similar densities [27,35].

Figure 6 shows the colloid-polymer-center-of-mass radial distribution function for $\sigma_c = 8$ at $q_r = 1$ (main plot) and $q_r = 4$ (inset). At low q_r, significant correlation, extending relatively far into the bulk, is observed along the colloid-rich branch of the binodal reminiscent of Fig. 4. As q_r is increased to 4 ($M = 350$), such correlations are completely lost for polymers which do not engulf a colloid ($l > q_r/2 - d = 1.875$). When engulfment does occur, a clear separation of each half of the binodal at small separations becomes apparent. For the colloid-rich branch, the more compressed coils osmotically repel the colloid from the core of the polymer more strongly; extrapolating near the center of the coil to $g_{c,p}(l = 0) \approx 0.1$, while along the polymer-rich branch this rises to $g_{c,p}(l = 0) \approx 0.3$. This is, of course, approximate as the center of a coil is actually located at $l = -d$, which is not shown for clarity. As q_r crosses from the colloid to the protein limit, chain size is no longer a relevant length scale. Slowly giving way instead to the correlation length, the loss of significant correlations for $q_r \geqslant 4$ depicted in Fig. 6 is consistent with the previous observation [16] that critical point densities decay to a constant, finite limit above this macroscopic size ratio.

The potential of mean force (PMF) offers further insight. In Fig. 7 we show the results for $\sigma_c = 8$ for the tie line furthest from the critical point (points A and D). As expected, the polymer-rich branch of the binodal (filled symbols) is much more attractive at contact (nearly a factor of 2). However, the effective depletion potential is less than 1 k_BT along the opposite branch (open symbols). As q_r increases, we observe a counterintuitive decrease in the attractive force at contact, despite the fact that these systems are less stable and demix at lower colloid concentrations [16]. At long range, this trend reverses; along the colloid-rich branch the repulsive barrier is significantly lowered, and the polymer-rich portion becomes even more attractive, though the effect becomes less pronounced for $q_r > 2$. Given that significantly more structure exists at low q_r it is reasonable to expect short-range interactions to be stronger at $q_r = 1$, whereas the increasing magnitude of the longer range interaction with increasing q_r is responsible for the overall decrease in critical point densities as q_r increases. Figure 7 suggests the crossover occurs at $r \approx 1.2\sigma_c$. The inset of Fig. 7 contrasts the PMF near the critical point (tie line connecting points B and C); the effects are qualitatively the same with increasing q_r but at contact the force is weakened by 10%–20%. As the critical point is approached, the average contact PMF between each phase converges to -1 k_BT.

One major area of interest for colloid-polymer systems is estimating the effect dissolved colloids have on polymer dimensions. Different simulations and theories have previously predicted expansion, contraction, or little to no effect on polymer radii of gyration [38,41–45]. For the systems we studied, however, we find the chains are universally compressed. Figure 8 shows the ratio between the bulk radius of gyration and that predicted by the scaling result in Table I. It is clear that with increasing q_r and σ_c, the chains are progressively compressed as colloid density increases. Extrapolation to $\rho_c = 0$ suggests that chains are still compressed over their infinitely dilute dimensions; this is a consequence of the polymer mesh, which is sufficiently dense to begin screening out excluded volume effects between the monomers, reducing the Flory scaling exponent. This effect becomes more pronounced along binodals with larger colloid diameters (higher critical colloid

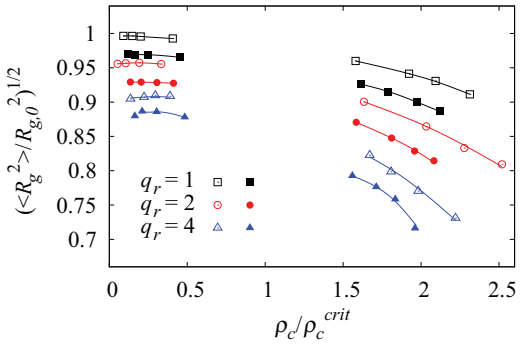

FIG. 8. (Color online) The ratio of the bulk radius of gyration to the known scaling for polymers on the fine lattice as a function of reduced colloid density along the binodals. Open and filled symbols denote measurements for $\sigma_c = 4$ and $\sigma_c = 8$, respectively.

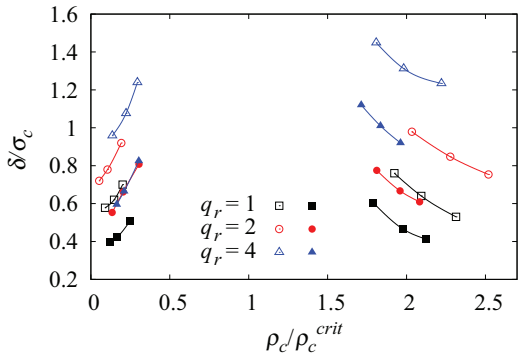

FIG. 9. (Color online) Monomer depletion radius around colloids as a function of reduced colloid density along the binodals. Open and filled symbols denote measurements for $\sigma_c = 4$ and $\sigma_c = 8$, respectively. Points nearest the critical point (B, C) are not depicted.

densities) and chain lengths, consistent with the previously discussed polymer coil osmotic compression mechanism.

Such observations are further supported by theory and simulations of coarse-grained polydisperse ideal polymers in the protein limit [42,43], which suggest that variability in polymer size can stabilize these systems against demixing. While these previous studies have focused on ideal polymers without explicit monomer-level detail, the introduction of an internal degree of freedom to account for polymer size variations due to polydispersity is akin to the size fluctuations due to internal rearrangements of a monodisperse species observed in this report. Remarkably we observe similar results. The trend in Fig. 8 suggests that with increasing colloid diameter, the chains are more compressed relative to their small particle counterparts; as shown previously [16], this is associated with a significant increase in the critical densities.

Finally, we consider the monomer depletion radius, that is, the radius around any given colloid from which the monomer is effectively absent [cf. Eq. (3)]. Coarse-grained descriptions of colloid-polymer solutions often employ an effective length scale of the *polymer* depletion radius and ignore effects on this smaller scale. This mean-field assumption ignores localized monomer order which could significantly contribute to polymer stability. Figure 9 illustrates two remarkable trends. First, with increasing q_r the depletion radius observed on both sides of the binodal increases, indicating an increasing propensity for monomer evacuation near the surface of the colloid, commensurate with the decrease in critical point densities as q_r is increased. It is also clear that with increasing d (smaller σ_c) the radius increases significantly, consistent with the solution's destabilization. The second observation is that as q_r increases an asymmetry develops between the two corresponding phases for both values of d. At $q_r = 1$, the depletion radius for each tie line is roughly equal in each phase for both d; however, δ increases significantly faster with q_r along the colloid-rich branch of the binodal than in the corresponding polymer-rich phase. For the latter phase, by the time q_r reaches 4 the radius slows its growth and begins to collapse. This asymmetry is due to the role-reversal first pointed out by Paricaud *et al.* [46]; in the protein limit, rather than the conventional idea of polymers depleting the colloidal species, instead the colloids may be thought of as the depletant for the polymers. As a result, as q_r increases rather than colloids partitioning between phases of similar polymer densities, the polymer instead begins to partition itself between phases with similar colloid densities. The expanding monomer depletion radius simply reflects this increased polymer partitioning.

At this point the significant destabilization previously observed on this lattice at sufficiently large d [16] still remains unexplained. We suggest the smaller colloid's instability can be rationalized by the emergence of a second, monomer-level depletion radius which destabilizes the solution at the onset of many-body interactions. Of course, given the freely jointed nature of our model polymer chain we may use the concept of "monomer" diameter and Kuhn length interchangeably here. Consider a simple monomeric depletion radius around the colloids to be on the order of the monomer diameter. Simple geometry reveals that the ratio of the monomer to colloid diameters at which three-body overlap of these layers begins to occur is $d \approx 0.1547$, or equivalently $\sigma_c \approx 6.5$. This limit falls nicely between the two diameters we have investigated, which separate the unstable regime ($\sigma_c < 6.5$) from the one where scaling nicely collapses the critical points [16]. This estimate of the monomer depletion radius is more of a "local" approximation than that reported in Fig. 9, which is significantly larger, simply because the latter is the result of integrated pair correlation functions and incorporates long range density fluctuations in surrounding "shells." It has been previously suggested that many-body effects may be responsible for increased immiscibility of smaller colloids due to overlapping many-bodied *polymer* depletion layers [22,23]; however, in this work we posit that many-body depletion on a monomeric level is a more satisfactory explanation, given that in the protein limit, polymeric depletion effects are felt at distances on the order of the polymer mesh's correlation length, which is much smaller than the polymer's overall dimensions. This is supported by the observation that the locations of structural features collapse *only* when the abscissa is linearly shifted by the monomer diameter (reduced distance, l), suggesting that there is an underlying effect at this length scale.

IV. CONTINUUM MODELS

Lattice colloids have an inherently coarse surface especially prevalent at low σ_c, which could introduce a steric interaction between surfaces that is not present in smooth, continuum models. Additionally, the impact of the lattice model's freely fluctuating bonds in determining structure in these solutions is unclear. In this section, we report the structure of two continuum space colloid-polymer models at the coexistence densities of the lattice model. Differences between the fixed-bond and free-bond models are expected to be significant in the crossover region between the colloid and protein limits where the characteristic length scale over which depletion acts shifts from the order of the chains' overall dimensions to the correlation length of the solution's polymer mesh. Although we exclusively report on $\sigma_c = 4$ in this section, the general trends are equally representative of the system with $\sigma_c = 8$ as well.

The most salient difference between the models is in the behavior of the chains' radii of gyration (cf. Fig. 10). In all cases, the free-bond model has an inherently larger absolute

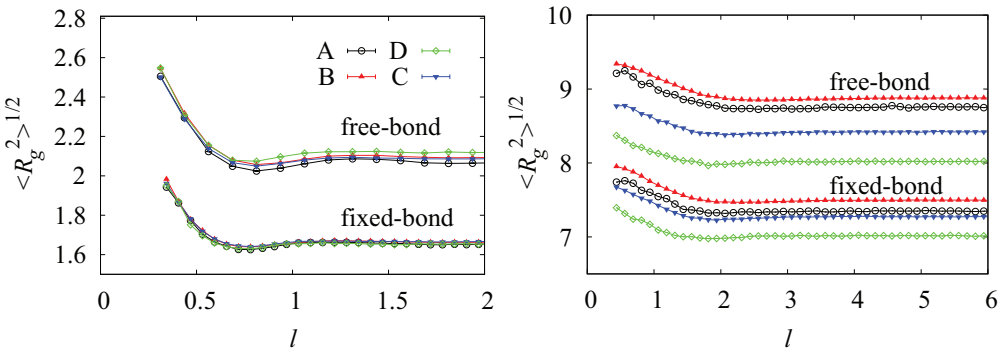

FIG. 10. (Color online) Average radius of gyration for polymers in continuum models at densities corresponding to lattice binodals for $\sigma_c = 4$, $M = 10$ (left, $q_r = 1$), 110 (right, $q_r = 4$). As M increases, both continuum models begin to show a weak density dependence, though the trend is clearly different from that observed on the lattice (cf. Fig. 5).

radius of gyration. At low q_r both models show relatively little density dependence; however, as q_r increases a separation between locations along the binodals becomes apparent. Both continuum models behave qualitatively the same, but exhibit significantly different trends with density than on the lattice (cf. Figs. 4 and 5). Along the colloid-rich branch of the binodals (A, B) the radii of gyration collapse more closely than along the polymer-rich branch (C, D), but not perfectly. Furthermore, the radii of gyration no longer monotonically vary with colloid density along the binodal curve as the lattice results did. As colloid density decreases in the colloid-rich phase (A to B), the chain is weakly expanded at all separations, while in the opposite polymer-rich phase, such a decrease (C to D) leads to chain compression. This effect is more noticeable with the free-bond model, but is not entirely absent from the fixed-bond model either. Care must be taken when drawing conclusions from these observations. The binodals for the continuum models are unknown, therefore a direct comparison of these results to those obtained on the fine lattice is not possible. We simply remark that both continuum models show similar qualitative behavior that is distinctly different from the lattice results.

More subtle differences are present in the second Legendre polynomial associated with the largest polymer semiaxis. For $q_r = 1$, the continuum models show no noticeable differences and results from the lattice in Fig. 4 are representative for the continuum models as well. At $q_r = 4$, the continuum models again show an approximate collapse along the colloid-rich branch (A, B) rather than the polymer-rich portion (C, D) of the binodal, unlike the lattice results. The range and magnitude of the orientational preference increase with colloid density. The fixed-bond model $P_{2,1}$ shows a minimum at $l \approx 1$, similar to the lattice model, though the magnitude is roughly half that observed in the latter. The free-bond model shows a bit more variability with a minimum ranging from $l \approx 1$–1.5, again with a much smaller magnitude than the lattice results. Finally, in both continuum models, the magnitude of the $P_{2,1}$ curve over the entire range of l is a monotonic function of colloid density, unlike the lattice model (cf. Fig. 5).

When Figs. 10 and 11 are compared to Figs. 4 and 5, it is clear that the lattice model is characterized by stronger short-range effects, while the continuum models tend to exhibit a weaker long-range influence on polymer structure. This observation is summarized in Fig. 12, which shows the weakening capacity of the polymer coils to repel colloids from their core as bonds "soften," with the correlation function approaching unity at shorter range moving from the free-bond to the lattice model. While it is beyond the scope of this paper to report extensively on the details of continuum results, it is important that these qualitative differences be mentioned to illustrate the nontrivial differences between lattice and

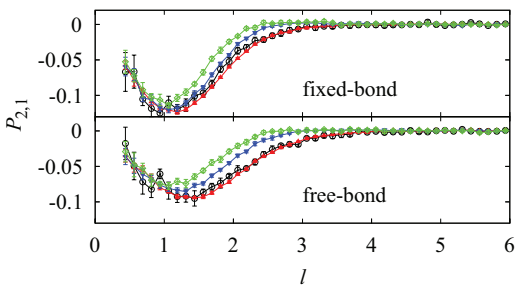

FIG. 11. (Color online) Second Legendre polynomial for a polymer's largest semiaxis in the case of $\sigma_c = 4$, $M = 110$ ($q_r = 4$). The magnitude of the features decays from top to bottom (fixed- to free-bond) while the range over which the colloids perturb the polymer increases in this order. Symbols are the same as in Fig. 10.

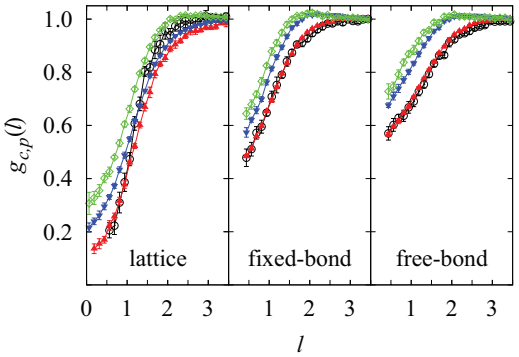

FIG. 12. (Color online) Colloid-polymer-center-of-mass pair correlation function for $\sigma_c = 4$, $M = 110$ ($q_r = 4$). Polymer wrapping increases from left to right. All curves approach unity beyond the range shown. Symbols are the same as in Fig. 10.

continuum models. Part of the differences may be due to our ignorance of the continuum binodal curves.

V. CONCLUSIONS

In this report, we investigated the structure of phase separated systems of athermal colloids and linear polymers in the protein limit. We reported the influence of two length scales: the macroscopic ratio, $q_r = 2R_g/\sigma_c$, and the microscopic ratio, $d = \sigma_s/\sigma_c$. For the lattice model, for which the binodals are known, we find that polymer size and orientation are strongly influenced by the location along the binodal. For all macroscopic size ratios we find that the bulk polymer is compressed weakly over its infinitely dilute size primarily due to excluded volumes between monomers in the polymer-rich phase, and strongly in the opposite phase primarily due to interaction with the colloids. Along the colloid-rich branch of the binodal for $q_r = 1$, polymers form up to three weakly structured "shells" of preferential size and orientation around the colloids, which weaken further into the bulk. In these shells, the polymer is distended and preferentially oriented normal to the surface of the colloid; these features are progressively weakened as q_r increases (for all d). Less stable phases with smaller colloidal species ($\sigma_c = 4$) compress the polymers over their infinitely dilute state relatively less than their more stable, large particle counterparts in both phases consistent with results for polydisperse ideal polymers, which suggest variability in polymer size is associated with more stable solutions [42,43].

We observed that structural features of these phase separated mixtures changed qualitatively little with colloid curvature (d); instead, the most significant differences appeared in the degree of chain dimension compression and the size of the monomer depletion radius. We further suggest the source of the instability with small colloidal species observed in Ref. [16] may be due to many-body effects on a monomer level. Structural features tend to collapse to consistent locations in terms of reduced distances, $l = (r - \sigma_s)/\sigma_c = r/\sigma_c - d$, which incorporates a linear shift by the monomer size, suggesting there are relevant interactions at this length scale. By this hypothesis, the emergence of three-body effects due to overlapping monomer depletion layers should appear at $\sigma_c \approx 6.5$; this provides a quantitatively accurate division between the unstable, small colloids ($\sigma_c = 4$) and the more stable, large colloids ($\sigma_c = 8$), where it has been previously shown that critical points may be collapsed to a universal curve [16].

Finally, we attempted to reconcile the differences between our $z = 26$ lattice model and continuum models with different bonding potentials, to examine the importance of the fine lattice's freely fluctuating bonds and relatively coarse colloidal surfaces. Results from the continuum models are qualitatively very similar and show only small quantitative differences from each other; these models reproduce some, but not most, of the features observed on the lattice. Without knowledge of the exact location of the binodals for the continuum models, it is not possible to draw a strong conclusion about the relative impact of these factors; it remains an open question for future work.

ACKNOWLEDGMENTS

This publication is based on work supported by grant CBET-1033155 from the US National Science Foundation. Barry Irick was supported by an REU grant from the Princeton Center for Complex Materials, a US National Science Foundation Materials Research Science and Engineering Center (Grant Number DMR-0819860).

[1] H. N. W. Lekkerkerker and R. Tuinier, *Colloids and the Depletion Interaction*, Lecture Notes in Physics, Vol. 833 (Springer, Dordrecht, 2011).
[2] P. J. Skrdla, Langmuir **28**, 4842 (2012).
[3] B. van den Berg, R. Wain, C. M. Dobson, and R. J. Ellis, EMBO J. **19**, 3870 (2000).
[4] D. Marenduzzo, K. Finan, and P. R. Cook, J. Cell Biol. **175**, 681 (2006).
[5] S. Asakura and F. Oosawa, J. Polym. Sci. **33**, 183 (1958).
[6] F. Oosawa and S. Asakura, J. Chem. Phys. **22**, 1255 (1954).
[7] A. Vrij, Pure Appl. Chem. **48**, 471 (1976).
[8] A. P. Gast, C. K. Hall, and W. B. Russel, J. Colloid Interface Sci. **96**, 251 (1983).
[9] H. N. W. Lekkerkerker, W. C. K. Poon, P. N. Pusey, A. Stroobants, and P. B. Warren, Europhys. Lett. **20**, 559 (1992).
[10] H. N. W. Lekkerkerker, Colloids Surf. **51**, 419 (1990).
[11] M. Dijkstra, R. van Roij, R. Roth, and A. Fortini, Phys. Rev. E **73**, 041404 (2006).
[12] P. G. Bolhuis, A. A. Louis, and J. P. Hansen, Phys. Rev. Lett. **89**, 128302 (2002).
[13] S. M. Ilett, A. Orrock, W. C. K. Poon, and P. N. Pusey, Phys. Rev. E **51**, 1344 (1995).
[14] E. J. Meijer and D. Frenkel, Phys. Rev. Lett. **67**, 1110 (1991).
[15] E. J. Meijer and D. Frenkel, J. Chem. Phys. **100**, 6873 (1994).
[16] N. A. Mahynski, T. Lafitte, and A. Z. Panagiotopoulos, Phys. Rev. E **85**, 051402 (2012).
[17] P. G. Bolhuis, E. J. Meijer, and A. A. Louis, Phys. Rev. Lett. **90**, 068304 (2003).
[18] G. J. Fleer and R. Tuinier, Phys. Rev. E **76**, 041802 (2007).
[19] G. J. Fleer and R. Tuinier, Adv. Colloid Interface Sci. **143**, 1 (2008).
[20] K. J. Mutch, J. S. van Duijneveldt, J. Eastoe, I. Grillo, and R. K. Heenan, Langmuir **25**, 3944 (2009).
[21] C. Chou, T. Vo, A. Z. Panagiotopoulos, and M. Robert, Physica A **369**, 275 (2006).
[22] M. Surve, V. Pryamitsyn, and V. Ganesan, J. Chem. Phys. **122**, 154901 (2005).
[23] V. Ganesan, C. J. Ellison, and V. Pryamitsyn, Soft Matter **6**, 4010 (2010).
[24] M. Fuchs and K. S. Schweizer, Europhys. Lett. **51**, 621 (2000).
[25] M. Fuchs and K. S. Schweizer, J. Phys.: Condens. Matter **14**, R239 (2002).
[26] J. B. Hooper, K. S. Schweizer, T. G. Desai, R. Koshy, and P. Keblinski, J. Chem. Phys. **121**, 6986 (2004).

[27] M. Doxastakis, Y.-L. Chen, O. Guzmán, and J. J. de Pablo, J. Chem. Phys. **120**, 9335 (2004).
[28] M. Doxastakis, Y.-L. Chen, and J. J. de Pablo, J. Chem. Phys. **123**, 034901 (2005).
[29] M. A. Annunziata and A. Pelissetto, Mol. Phys. **109**, 2823 (2011).
[30] D. Frenkel and B. Smit, *Understanding Molecular Simulation*, 2nd ed. (Academic Press, San Diego, 2002).
[31] "Hoomd-blue", http://codeblue.umich.edu/hoomd-blue.
[32] J. A. Anderson, C. D. Lorenz, and A. Travesset, J. Comput. Phys. **227**, 5342 (2008).
[33] D. N. LeBard, B. G. Levine, P. Mertmann, S. A. Barr, A. Jusufi, S. Sanders, M. L. Klein, and A. Z. Panagiotopoulos, Soft Matter **8**, 2385 (2012).
[34] D. M. Heyes and H. Okumura, J. Chem. Phys. **124**, 164507 (2006).
[35] R. C. Picu and M. S. Ozmusul, J. Chem. Phys. **118**, 11239 (2003).
[36] T. Pakula, J. Chem. Phys. **95**, 4685 (1991).
[37] M. R. Shaw and D. Thirumalai, Phys. Rev. A **44**, R4797 (1991).
[38] P. van der Schoot, Macromolecules **31**, 4635 (1998).
[39] M. Rubinstein and R. H. Colby, *Polymer Physics* (Oxford University Press, New York, 2003).
[40] H. W. H. M. Janszen, T. A. Tervoort, and P. Cifra, Macromolecules **29**, 5678 (1996).
[41] M. Vacatello, Macromolecules **35**, 8191 (2002).
[42] A. R. Denton and M. Schmidt, J. Phys.: Condens. Matter **14**, 12051 (2002).
[43] B. Lu and A. R. Denton, J. Phys.: Condens. Matter **23**, 285102 (2011).
[44] D. Antypov and J. A. Elliott, Macromolecules **41**, 7243 (2008).
[45] Q. W. Yuan, A. Kloczkowski, J. E. Mark, and M. A. Sharaf, J. Polym. Sci., Part B: Polym. Phys. **34**, 1647 (1996).
[46] P. Paricaud, S. Varga, and G. Jackson, J. Chem. Phys. **118**, 8525 (2003).